Dysprosium-doped silica fiber as saturable absorber for mid-infrared pulsed all-fiber lasers

Pascal Paradis, Tommy Boilard, Vincent Fortin, Stanislaw Trzesien, Michèle Ude, Bernard Dussardier, Réal Vallée, Martin Bernier

Research Article Vol. 30, No. 3 / 31 Jan 2022 / Optics Express 3367
Optics EXPRESS

Dysprosium-doped silica fiber as saturable absorber for mid-infrared pulsed all-fiber lasers

PASCAL PARADIS,[1,*] TOMMY BOILARD,[1] VINCENT FORTIN,[1] STANISLAW TRZESIEN,[2] MICHÈLE UDE,[2] BERNARD DUSSARDIER,[2] RÉAL VALLÉE,[1] AND MARTIN BERNIER[1]

[1] *Center for Optics, Photonics and Lasers, Université Laval, Québec, Canada*
[2] *Université Côte d'Azur, CNRS, Institut de Physique de Nice, Nice, France*
[*] *pascal.paradis.2@ulaval.ca*

Abstract: We report on a mid-infrared Q-switched erbium-doped all-fiber laser using a dysprosium-doped silica fiber as saturable absorber for the first time in this wavelength range. Moreover, we demonstrate the use of a highly reflective chirped fiber Bragg grating written in a silica fiber as the input coupler for such lasers. This Q-switched all-fiber laser generates a stable pulse train centered at 2798 nm with a maximum average power of 670 mW at a repetition rate of 140 kHz with a pulse duration of 240 ns and a pulse energy of 4.9 µJ.

1. Introduction

In the last decade, there has been a significant effort to develop both fluoride and chalcogenide mid-infrared (mid-IR) lasers due to their potential for addressing a growing number of applications [1,2]. It is well known that many biological and organic molecules that are closely related to our environment, industries and health possess strong fundamental absorption peaks in the mid-IR wavelength range known as the molecular fingerprint region. It is more energy efficient to use a mid-IR laser tuned on specific and strong fundamental absorption peaks of materials for spectroscopy, material processing and medical applications. For example, since the absorption peak of liquid water is at 2940 nm, using a laser operating near this wavelength for surgery would ensure a very accurate cutting line with much less damage to the peripheral tissues while being much more energy efficient. Another example of application that would benefit from the use of a mid-IR laser is the remote sensing of atmospheric pollutants such as methane or carbon dioxide.

Up to now, demonstrations of mid-IR fiber lasers have shown their great potential for those applications [1–3]. However, despite their improved performances and their broad range of pulse specifications, most of the mid-IR Q-switched or mode-locked fiber lasers reported so far have a common weakness that makes them difficult to deploy in field applications i.e., they are not all-fiber due to the lack of commercial fiberized components (such as optical isolators, wave plates, polarizers and saturable absorbers) available in the mid-IR wavelength range [4–14]. A crucial step towards democratizing the use of mid-IR pulsed fiber lasers for field applications is in fact to address the lack of robust fiberized components for the mid-IR, starting with the saturable absorbers (SA). To this extent, multimode interference using a multimode optical fiber as SA could be an option, but it would be difficult to make such an all-fiber laser cavity since the length and the core-to-core alignment of the multimode fiber are critical for its proper operation and the splicing of fluoride fibers is much more involved than that of silica fibers [15]. So far, there are two demonstrations of mid-IR pulsed fiber lasers that did not involve free-space propagation: one is a gain-switched all-fiber laser using the simplicity and robustness of CW all-fiber lasers' design [16], and the other one is a Q-switched mode-locked almost all-fiber laser design using homemade butt-coupled MXene and $PtSe_2$ flat SA [17].

#448060 https://doi.org/10.1364/OE.448060
Journal © 2022 Received 9 Nov 2021; revised 4 Jan 2022; accepted 5 Jan 2022; published 18 Jan 2022

Optics EXPRESS

Several absorbing doped fibers have been studied for implementing Q-switched all-fiber lasers in the near IR at 1.0, 1.55 and 2.0 μm [18]. In principle, good SAs shall have a strong absorption cross section and a short (around μs or less) relaxation time. In this aim, 3d transition metals such as chromium (IV) in silica fiber have been investigated in first all-fiber Q-switched 1 μm lasers [19,20]. The use of rare-earth elements as SAs , such as samarium [21], or holmium [22,23], have shown limitations because of low saturation fluence, mainly due to low saturation intensity, long response time and complex setup to artificially shorten the SA response. Fiber SAs for the mid-IR domain would benefit from the very strong absorption of transition metals, such as Cr^{2+}, but to our knowledge no fiber SA was developed using this element. Also some rare-earth elements have mid-IR transitions. Dy^{3+} is one of the most promising rare earth ions to act as fiber-based SA with an optical absorption transition around 2.8 μm. Furthermore, using silica as a host matrix in an all-fiber SA will provide a short relaxation time given the quite high phonon relaxation rate of silica for mid-IR transitions.

In this paper, we demonstrate the use of a dysprosium-doped silica fiber as a SA for the first time in a Q-switched all-fiber laser emitting at 2798 nm. Another novel aspect of this demonstration is the highly reflective chirped fiber Bragg grating (FBG) written in a silica fiber used as the input coupler of this laser cavity.

2. Silica fibers' fabrication and characteristics

The silica-based fibers were manufactured at *Institut de Physique de Nice*. The fibers (cladding diameter of 220 μm, core diameter of 15 μm and NA of 0.12) were drawn from a preform manufactured by Modified Chemical Vapor Deposition (MCVD) and the recently home-developed "gradual solution doping method" [24]. It was used to prepare a series of fiber samples from a sole preform with gradual concentrations of the rare-earth oxides La_2O_3 and Dy_2O_3 along its length, whereas the concentration in the glass modifier Al_2O_3 remained constant. A porous silica layer was deposited inside a pure silica substrate tube (*Heraeus*, F300). First, the porous layer was soaked for a set time by filling the substrate tube with an ionic solution of aluminum trichloride and lanthanum trichloride in ethanol. After emptying the tube from the first solution, a second ionic solution of aluminum trichloride and dysprosium trichloride in ethanol was immediately injected up to approximately half of the substrate tube height. During this second soaking period, the initially adsorbed La^{3+} ions were gradually desorbed from the porous layer into the second solution, and were replaced by Dy^{3+} ions. After a set soaking time, the solution was drained, and the porous layer was dried, oxidized and sintered into a doped silica layer [25]. The substrate tube was collapsed into a solid preform of a typical external diameter of 9.5 mm and core diameter of 0.75 mm. Due to various effects comprising liquid surface tension, porous layer wettability, ionic diffusion and adsorption/desorption dynamics during the soaking phases, the core of the preform had a continuous and gradual decrease of La_2O_3 content from 0.2 mol% down to less than 0.01 mol% together with an increase of Dy_2O_3 from 0.005 mol% to 0.21 mol% (Table 1, Fig. 1). The NA of the fiber is constant within ±5% over the compositional varying length. This technique allows to freely choose the unsaturated absorption coefficient of the SA. Also, as lanthanum is physically and chemically similar to dysprosium, both rare-earth substitute to each other in the glass network. This has a "dilution effect" on the optically active rare-earth elements, and hence mitigates unwilled interaction clusters of dysprosium atoms.

The chemical composition of the silica fibers presented in Table 1 has been measured with an electron microprobe in the vicinity of their respective core and Fig. 1 shows the distribution of the elements doped into the core of the fibers. Since both fibers were drawn from the same preform manufactured by gradual solution doping, some traces of Dy^{3+} ions may be present in the non-Dy^{3+}-doped silica fiber, though it is not significant and close to the microprobe limit of detection, as can be seen in Fig. 1. Given that this silica fiber doesn't contain a significant amount of dysprosium ions, we refer to it as "undoped" in the remaining text of this paper as opposed

Optics EXPRESS

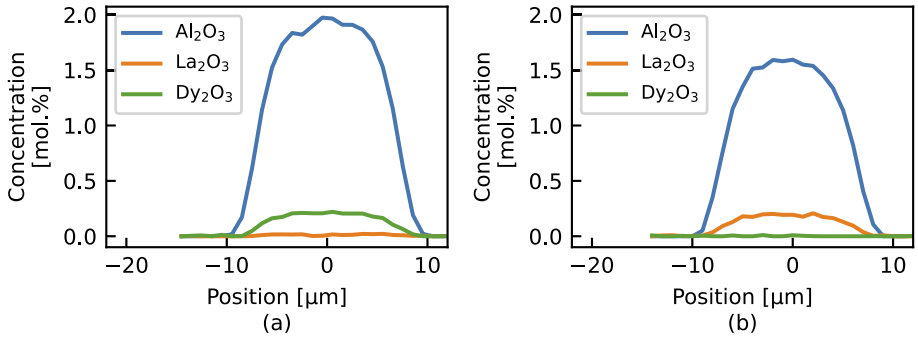

Fig. 1. Comparison of the core's composition of (a) the Dy^{3+}-doped and (b) the "undoped" silica fibers as measured by electron microprobe analysis.

Table 1. Measured composition of the core of the Dy^{3+}-doped and the "undoped" silica fibers

	Concentration [mol.%]			
Fiber	SiO_2	Al_2O_3	La_2O_3	Dy_2O_3
Dy^{3+}-doped silica fiber	97.878	1.901	0.012	0.209
"undoped" silica fiber	98.226	1.572	0.197	0.005

to the saturable absorber that is the Dy^{3+}-doped silica fiber. The refractive index profiles of both Dy^{3+}-doped and "undoped" fibers (not shown) follow the typical bell-shaped composition distribution as shown in Fig. 1 since Al_2O_3, Dy_2O_3 and La_2O_3 are index risers in silica. The core diameter at half maximum of the refractive index profile is 15 μm.

The transmission of both silica fibers shown in Fig. 2 has been measured with a "cut-back" technique using a homemade low-power supercontinuum source. It can be seen that the transmission around 2800 nm of the "undoped" silica fiber is about −20 dB/m, which transposes to 0.8 dB for a cavity round trip in two centimeter length as used in the demonstrated laser design. This transmission is comparable to what is reported in the literature [26] and about 1000 times lower than the transmission of the erbium-doped fluoride glass fiber [27]. As for the losses of the Dy^{3+}-doped silica fiber, they are much more significant, i.e., slightly in excess of 100 dB/m around 2800 nm. Based on this high absorption, a short length of this fiber is sufficient to act as SA. Note that the absorption peak of the latter fiber is centered around 2740 nm which is really close to the fundamental absorption peak of -OH group centered at 2720 nm in silica [28]. However, we estimated an OH concentration of 1.2±0.4 ppm from an absorption peak at 1380 nm. This would lead to a non-saturable absorption of about 12 dB/m at 2720 nm according to [28]. This 2740 nm absorption peak is also much less intense in the "undoped" silica fiber while still being produced with the same solution doping process. It should be noted that to ensure the proper guiding of the pump through the cladding of this fiber, they were stripped of their original non-guiding protective coating and recoated with low refractive index polymer (fluoroacrylate, n=1.33) in the all-fiber cavity.

Silica glass was chosen as the host material for the dysprosium ions for its significantly higher phonon energy compared to fluoride glass. The energy gap of the Dy^{3+}:$^6H_{13/2}$ - $^6H_{15/2}$ optical transition is around 3600 cm^{-1}. In silica, only 3 phonons (1100 cm^{-1}) suffice to span this energy gap down, at an estimated rate of 5×10^5 s^{-1} [29]. Hence the relaxation from the upper energy multiplet is almost fully driven by non-radiative decay (NRD). The lifetime is estimated to be around 2 μs at most [30], that is a sought relaxation time for an efficient SA [31]. Hence using silica ensures a much shorter lifetime than the fluoride glass one of 630 μs [32]. Exploratory

Optics EXPRESS

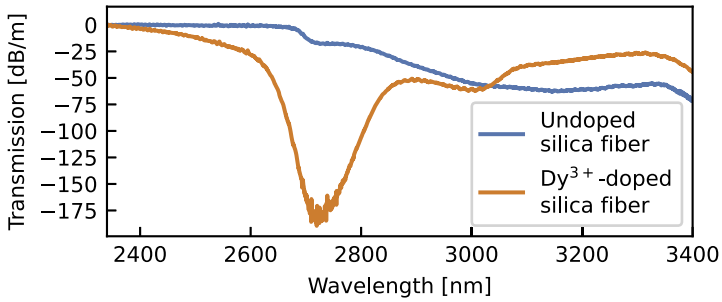

Fig. 2. Mid-infrared transmission of the Dy^{3+}-doped and the "undoped" silica fibers

numerical simulations showed that Dy^{3+}-doped fluoride fiber would simply be saturated and no pulses would be generated. Actually, according to these simulations, an upper level's lifetime longer than 3 µs would lead to CW emission. Moreover, the dysprosium ions in the silica glass matrix are more prone to form clusters of ions than in fluoride glass, further shortening the non-radiative decay rate. From the same numerical simulations using an upper level's lifetime of about 300 ns showed a Q-switching behavior similar to what is observed experimentally in this demonstration. We tried to measure the saturable absorption (modulation depth) and the saturation fluence of the Dy^{3+}-doped silica fiber using a setup similar to the one described in [33], but we could not observe saturation effects. Either the attenuation of the pulsed laser source was too limited or the power of the laser source itself was not suitable to measure the saturation phenomenon. The characterization of this saturable absorber is in progress. However, as can be deducted from the Q-switched behavior reported in this paper, the Dy^{3+}-doped silica fiber is indeed acting as a SA.

3. Q-switched fiber laser experiments and results

To characterize the behavior of this laser cavity design, two versions of the experimental setup were studied: a first one involving free-space propagation to ease the optimization of the length of the dysprosium-doped silica fiber in the laser cavity and a second one with a robust and optimized all-fiber design to demonstrate its feasibility and to assess its current limitations. Throughout this demonstration, all the aspheric ZnSe lenses are AR coated and have a transmission of about 95% near 2800 nm. The average output power is measured using a thermopile detector (*Gentec-eo*, XLP12-3S-H2-D0), while the laser emission spectrum is acquired with a grating based optical spectrum analyzer (OSA) (*Yokogawa*, AQ6376) and the pulse train is acquired by a 200 ps rise-time InGaAs detector (*Alphalas*, UPD-5N-IR2-P). The same OSA is used to measure the transmission spectra of the silica fibers and FBGs.

3.1. Free-space setup to optimize the SA configuration

The schematic of the free-space setup to optimize the SA configuration is shown in Fig. 3. This laser cavity is backward pumped by a 976 nm diode (*BWT*, K976DB2RN-10.00W) to keep the other end of the laser cavity free for optimizing the dysprosium-doped silica fiber length. The laser beam coming out of the 105 µm pigtailed multimode fiber of the pump diode is launched into the cladding of the gain fiber. This gain fiber is a 2.5 m-long 7 mol.% erbium-doped fluoride fiber (*Le Verre Fluoré*) that has a core diameter of 15 µm and a numerical aperture (NA) of 0.12, and a double D-shaped cladding with a diameter of 240×260 µm and a NA of 0.5. The fluoride fiber's tip is angle cleaved at 6.5° and the dysprosium-doped fiber's tip is also angle cleaved at around 5° for each tested length to avoid parasitic Fresnel reflections. The FBG has a maximum reflectivity of 70 % centered at 2791 nm with a full width at half maximum (FWHM)

Optics EXPRESS

of 3.0 nm and is written in the core directly through the coating of the active fiber to preserve the physical integrity and thus the robustness of the fiber [34]. To improve the stability of the setup and ensure the same experimental conditions especially when shortening the silica fiber's length, the fluoride fiber is spliced directly to the Dy^{3+}-doped silica fiber using a Thorlabs Vytran GPX system with an iridium filament. The fusion splice between these two fibers is somehow tricky because molecular bonding is difficult to achieve with such dissimilar glass materials. Splicing is therefore accomplished by first heating the silica fiber to a prescribed temperature and then pushing it into the fluoride fiber to form a grasping bulge as the fluoride glass cools down, due to the different thermal expansion coefficients of the silica and fluoride glasses [35]. Such splice could withstand a tension test of 500 gf. Similar splices were shown to last for several months at room temperature and also to withstand temperature cycling over 36 hours between 25°C and 100°C. The silica fiber was fabricated at the *Institut de Physique de Nice* as described in section 2., and its geometry and guiding properties (cladding diameter of 220 µm, core diameter of 15 µm and a NA of 0.12) were chosen to mode match with the fluoride fiber and thus to optimize splice transmission. A transmission of 78% was obtained (as measured at 2000 nm because the dysprosium fiber is strongly absorbing near 2800 nm), which revealed sufficient for efficient Q-switched lasing although higher transmission could likely be achieved with an optimized splicing process. The residual pump power which is significant despite the cladding mode stripper (CMS) is removed by the dichroic mirror inside the laser cavity. This dichroic mirror is also used to compare the behavior of this laser cavity without the Dy^{3+}-doped silica fiber but with a SESAM in place of the gold mirror in the same cavity design as in [7].

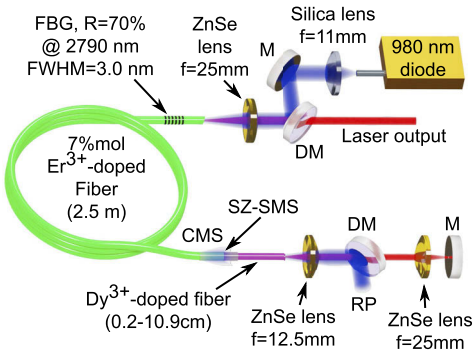

Fig. 3. Schematic of the free-space cavity used to characterize the effect of the dysprosium-doped silica fiber length on the pulses characteristics (CMS: cladding mode stripper; DM: dichroic mirror; M: gold mirror; FBG: fiber Bragg grating; HR: high reflectivity; LR: low reflectivity; RP: residual pump; SZ-SMS: silica-ZrF_4 single mode splice)

The free-space cavity exhibited a Q-switching behavior whereas no mode locking was observed under the present experimental conditions. However, it should be noted that before splicing the Dy^{3+}-doped silica fiber to the gain fiber, this laser cavity emitted in CW regime without any pulse whatsoever when no SA was present in the laser cavity and it emitted in mode-locked regime when the intracavity gold mirror was replaced with a SESAM (BATOP GmbH) as in [7]. Hence, the Dy^{3+}-doped silica fiber definitely acts as SA. Since the absorption of the SA is volumic, the effect of the length of the Dy^{3+}-doped silica fiber was first studied using this free-space cavity. Figure 4 is summarizing this analysis in terms of the laser parameters, including the output power, the repetition rate, the pulse duration and pulse energy. As shown in Fig. 4(a) and (b), it appears that the lasing efficiency and the repetition rate are, as expected, both increasing with shorter SA lengths. However, shortening the Dy^{3+}-doped silica fiber beyond some point seems to result in longer pulse duration and slightly smaller maximum pulse energy as can be seen in Fig. 4(c) and

Optics EXPRESS

(d). The energy required to saturate the whole length of the Dy^{3+}-doped silica fiber can explain this behavior since if more energy is needed, it means that there is also more energy stored in the gain fiber causing it to have a shorter pulse build-up time once the SA is saturated. With 2 mm of Dy^{3+}-doped silica fiber, the maximum average output is 667 mW at 232 kHz with a pulse duration of 337 ns and a pulse energy of 2.9 µJ. However, if the length of the SA is too long, then its non-saturable losses become significant and lower is the extracted energy from the laser cavity. With 10.9 cm of Dy^{3+}-doped silica fiber, the maximum average output is 81 mW at 92 kHz with a pulse duration of 258 ns and a pulse energy of 0.88 µJ. So, the optimal SA length is found to be at most a few centimeters but more than a few millimeters. From this particular data set, the Dy^{3+}-doped silica fiber's optimal length is 26 mm for optimizing the pulse duration while generating a high pulse energy: maximum average power of 405 mW at 119 kHz with a pulse duration of 230 ns and a pulse energy of 2.3 µJ. For every studied length, the Q-switched regime threshold was the same as the lasing threshold and the laser output remained in a stable Q-switched regime from its onset to the highest pump power available from the diode used in the free-space cavity.

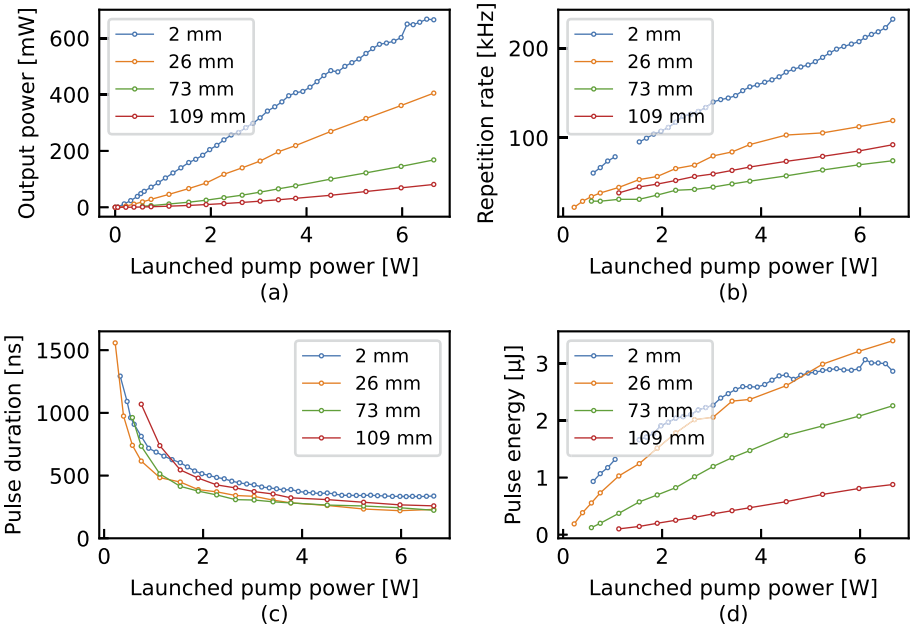

Fig. 4. Performance of the free-space cavity, i.e. (a) laser curve, (b) repetition rate, (c) pulse duration and (d) pulse energy as a function of the injected pump power, according to the length of the Dy^{3+}-doped silica fiber in the free-space cavity.

3.2. *Optimized all-fiber laser setup*

Realizing that the Q-switching threshold was as low as the lasing threshold while using a rather strongly reflective output coupler in the free-space cavity, we decided to switch to the all-fiber laser cavity as depicted in Fig. 5 in order to study the effect of the output coupler's reflectivity on the behavior of this laser. In this all-fiber laser, the gain fiber is forward pumped by a more powerful 30 W 976 nm diode (*II-IV*, BMU30-975-01-R). The pump diode's pigtailed multimode silica fiber is spliced to the silica fiber containing the HR-FBG (input coupler). The remaining length of "undoped" silica fiber located inside the laser cavity is about 2 cm. The "undoped" silica fiber is then spliced to the Dy^{3+}-doped silica fiber acting as the SA and these two fibers

Optics EXPRESS

are mode matched, thus resulting in splice transmission in excess of 95%. The length of the Dy^{3+}-doped silica fiber in this setup is 3.5 cm due to practical limitations, but it should be noted that a shorter and more optimal length could be achieved by perfecting the splicing recipe. The 80% transmission of this silica-ZrF_4 single mode splice was about the same as the one in the free-space cavity. The 3.5 m-long gain fiber is also a 7 mol.% erbium-doped fluoride fiber from *Le Verre Fluoré* with the same properties as in the free-space cavity. Both FBGs are written directly through the protective coating of their respective fiber using the same technique as for the free-space cavity. However, the HR-FBG written in the silica glass is also chirped to get a broad and highly reflective spectrum that overlaps more easily with the narrow reflection spectrum of the low reflective FBG (LR-FBG) written in the fluoride fiber. This ensures the proper operation of the laser cavity even if the HR-FBG or the LR-FBG shifts a little and made their production a bit easier because their design wavelength is less critical. Making these two FBGs centered around the same wavelength revealed challenging because of the different effective index of both fibers. However, the different range of possible refractive index modulation in the silica and fluoride fibers helped with the writing of the FBGs for this laser cavity. The laser emission wavelength is prescribed by the LR-FBG's narrower reflectivity peak as seen in Fig. 6. The output tip of the fiber is also angle cleaved at 5° to avoid parasitic feedback. The residual pump is separated from the 2800 nm laser output beam with the same dichroic mirror as in the free-space cavity in order to monitor the laser output and the residual pump at the same time. However, it should be noted that the free-space optical components (the lens and the dichroic mirror) are outside of the laser cavity. The dichroic mirror could easily be replaced by a cladding-pump stripper in further setups where the characterization of the residual pump is not necessary.

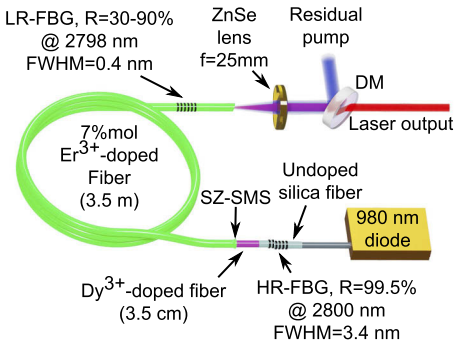

Fig. 5. Schematic of the all-fiber cavity used to demonstrate the feasibility of a mid-IR Q-switched all-fiber laser using this Dy^{3+}-doped silica fiber as SA as well as the limitations of such a laser design. (CMS: cladding mode stripper; DM: dichroic mirror; M: gold mirror; FBG: fiber Bragg grating; HR: high reflectivity; LR: low reflectivity; SZ-SMS: silica-ZrF_4 single mode splice)

The LR-FBG in this setup was written specifically to be able to lower its reflectivity from 90% to 30% by progressively heating it by increments of 10 °C for 10 minutes from 80 °C up to 190 °C. At this last temperature, the peak of the laser emission spectrum shifted by 0.1 nm compared to the previous steps, so the LR-FBG could not be heated further to lower its reflectivity while keeping a similar laser emission spectrum for comparison purposes. Once again, the Q-switching threshold is the same as the lasing threshold for every output coupler's reflectivity and pulses are observed as soon as the power is high enough so that the pulse train can effectively be measured by the photodiode. Figure 7 shows the performances of this all-fiber laser cavity. Until the minimum reflectivity of 30% was achieved with this LR-FBG, the maximum power of the laser was limited to avoid any damage that would have prevented further characterization of the laser

Optics EXPRESS

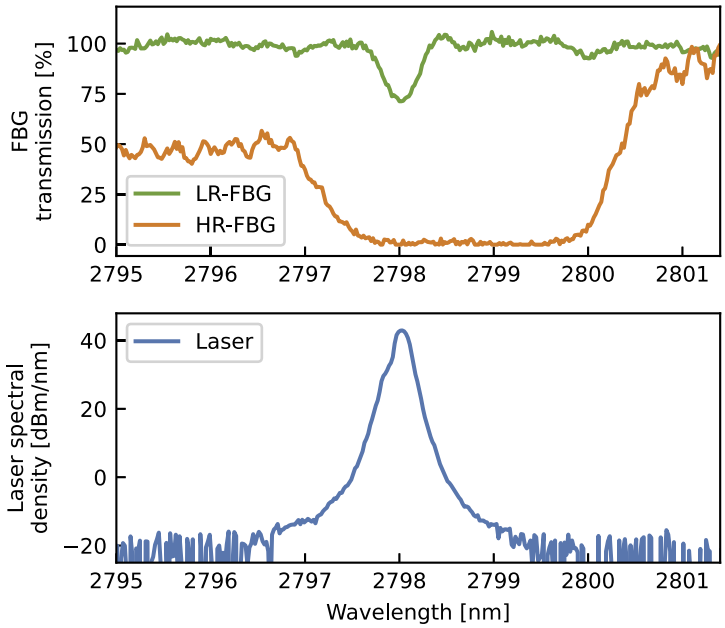

Fig. 6. The all-fiber cavity's FBGs' transmission spectra and 2798 nm laser emission spectrum as measured with the LR-FBG's peak reflectivity at 30% and a maximum absorbed pump power of 9.4 W

cavity in its optimal configuration. The temperature of the silica-ZrF_4 splice was also monitored to ensure safe operation of the laser until the minimum LR-FBG's reflectivity was achieved. However, for this last reflectivity point, proper thermal management of this critical splice was put in place by glueing it to a heat sink with a fan, and the pump power and output power were increased until the failure of the laser cavity. As expected, the best performance is obtained at the lowest LR-FBG's reflectivity for every given value of pump power. At its best, this mid-IR Q-switched all-fiber laser produced a maximum average power of 670 mW at a repetition rate of 138 kHz with a pulse duration of 238 ns, a pulse energy of 5 µJ and a peak power of 17.5 W. The maximum pump power launched into the gain fiber was 11.7 W with 2.35 W of residual pump power. The maximum lasing efficiency according to the absorbed pump power is 8.9% despite the use of about 5.5 cm of silica fiber in the laser cavity as well as two intracavity single mode splices. It is more than 5 times the lasing efficiency obtained with the 90% output coupler's reflectivity. Since the Q-switched pulses are quite long, the chirp of the HR-FBG doesn't have a significant impact on their minimal duration. The heating of the Dy^{3+}-doped silica fiber at high power actually resulted in the failure of the laser cavity from an increase of the loss of the silica-ZrF_4 splice due to thermomechanical effects.

Figure 8 presents the pulse train and zoom-ins on two consecutive pulses at the maximum average output power of 670 mW emitted by the all-fiber cavity. The Q-switched pulses exhibit self-mode-locked resembling substructures, which are very likely to result from mode beating of the cavity longitudinal modes, like those reported in typical gain-switched fiber lasers [16,36]. Those rapidly varying temporal patterns are changing from pulse to pulse which explains the large modulation of the measured pulse train's peak power with a standard deviation of 8% over 500 µs. To get a better visualization of the averaged pulse envelope, the mode-beating features in the temporal trace are filtered out with a moving average corresponding to a convolution of the temporal signal with a normalized gaussian function having a FWHM of 75 ns which corresponds to twice the mode-beating period of 35 ns (i.e., the laser cavity round-trip time).

Optics EXPRESS

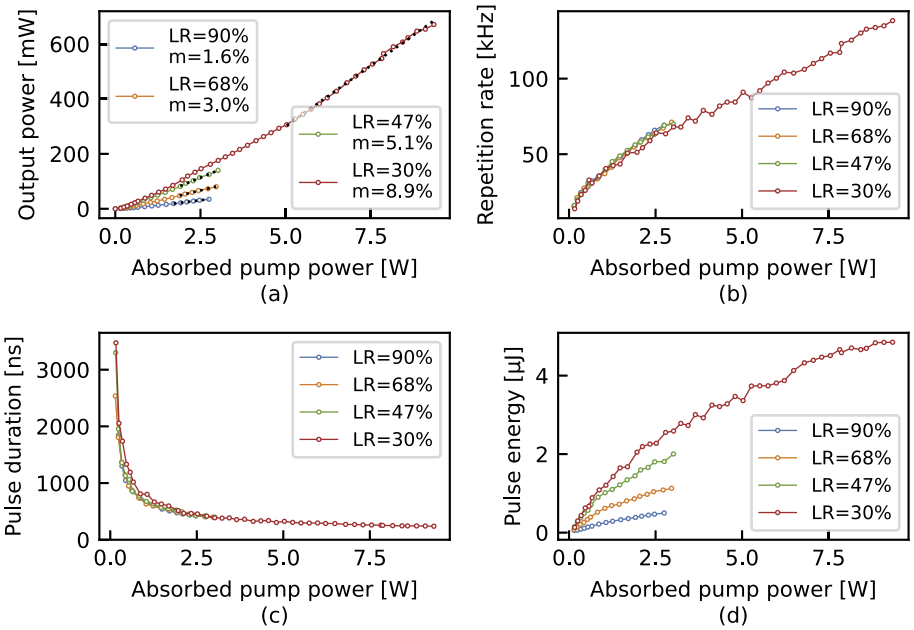

Fig. 7. Performance of the all-fiber cavity laser cavity, i.e. (a) laser curve, (b) repetition rate, (c) pulse duration and (d) pulse energy as a function of the absorbed pump power, according to the LR-FBG's peak reflectivity in the all-fiber cavity. The black dashed lines in (a) represent the lasing efficiency (m) of their respective laser curve.

The standard deviation of the energy per pulse (area under the pulse's curve) was evaluated from both the moving-averaged and the as-measured traces and a similar value of 3.5% was obtained in both cases. As for the standard deviation of the pulse duration, it was negligibly small i.e., on the order of the time sampling interval. Based on this, we calculated that the standard deviation of the moving-averaged pulse peak power is also 3.5%. Similar stability is observed at every power level.

3.3. Discussion

Comparing the performances of both laser cavities, we can conclude that the length of the SA in the all-fiber cavity seems a little too long to achieve the optimal performances. The lasing efficiency could have been better with a slightly shorter SA while also reducing the pulse duration a little. The peak power would also have been a little higher with about 2.5 cm of Dy^{3+}-doped silica fiber instead of the 3.5 cm that were used in the all-fiber cavity. Moreover, the pulse duration could also have been shortened by reducing the length of the laser cavity, i.e., using a shorter gain fiber, since the pulse's build-up time would have been shorter due to the higher pumping rate necessary to saturate the SA. The photon's round trip time inside the laser cavity would also have been shorter, further minimizing the pulse duration. Furthermore, a shorter length of silica glass fiber inside the laser cavity would have improved even more the overall performances of the all-fiber cavity by lowering the non-saturable losses inside the laser cavity. The forward pumping in the all-fiber cavity compared to the backward pumping in the free-space cavity is another significant difference that affects the performances of the all-fiber cavity. Using a pump combiner [37] to launch the pump power into the gain fiber from the output end would have yielded a slightly better average output power, higher pulse energy and also most probably a shorter pulse duration due to having to pump a bit more to get the same signal power and energy in the SA. However, such optimization was not necessary to demonstrate the viability of this

Optics EXPRESS

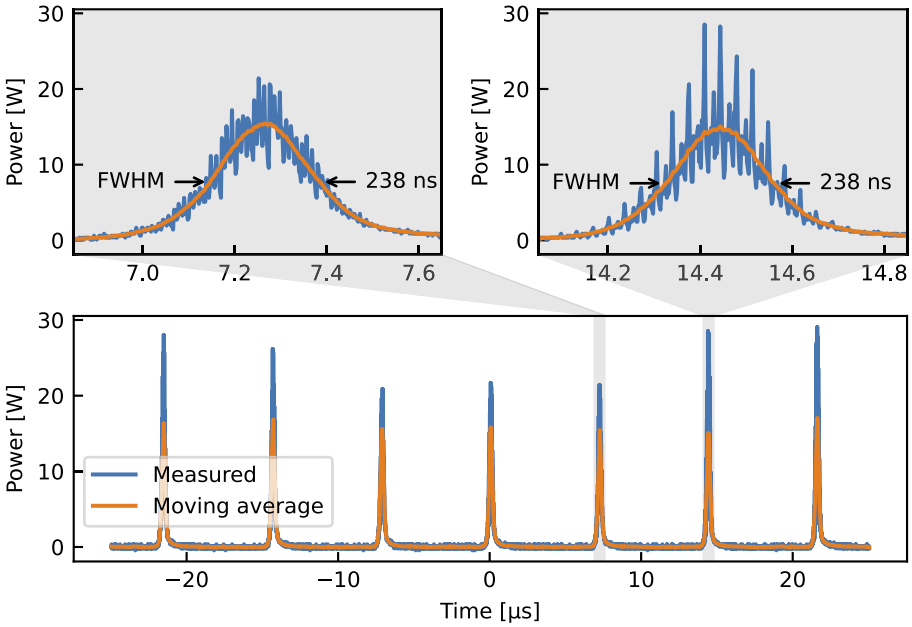

Fig. 8. (Bottom) Pulse train and (top) zoom-ins on two consecutive pulses at 670 mW of average power and 138 kHz with the LR-FBG's reflectivity at 30% in the all-fiber cavity

Q-switched laser system, its behavior and its limitations. So, we decided to keep every splice that had a good enough transmission as long as every component's length was close enough to their respective optimal length.

To mitigate the thermomechanical failure of the single-mode splice between the silica and fluoride fibers at high power, a very short "undoped" silica fiber could be spliced in between the fluoride fiber and the Dy^{3+}-doped silica fiber in order to avoid this problem in future experiments. It should also be noted that power scaling is still possible since there is no sign of saturation in the output power curve, and a LR-FBG with a lower peak reflectivity would allow for an even better lasing efficiency. Moreover, despite having much more pump power going through the cladding of the Dy^{3+}-doped silica fiber in the all-fiber cavity than in the free-space cavity, there were no apparent adverse effects on the performances of the SA as well as of the whole laser cavity.

As presented earlier, we were not able to observe any sign of a mode-locked regime from our cavities. We believe this is because the relaxation time of our saturable absorber is too long (estimated by modeling to be in the order of a few hundreds of nanoseconds) compared to the cavity round-trip time of 35 ns. To potentially enable mode locking, the saturable absorber's relaxation time could be reduced by increasing its dysprosium concentration to increase the rate of cross relaxations or by using a glass host with a larger phonon energy to increase non-radiative relaxations.

4. Conclusion

We demonstrated the first mid-infrared Q-switched all-fiber laser emitting at around 2800 nm based on a Dy^{3+}-doped silica fiber as SA. We also demonstrated that a highly reflective chirped FBG written in a silica fiber could be used in a mid-infrared all-fiber laser without hampering its efficiency. Despite the use of silica fibers inside this mid-infrared laser cavity, the lasing efficiency according to the absorbed pump power is still good at 8.9%. This kind of rare-earth-doped silica fiber could be used in other mid-infrared fiber lasers provided that the total length of

Optics EXPRESS

silica fiber inside the laser cavity is optimized to manage its non-saturable losses. Finally, the improved robustness, reliability and damage threshold provided by such a fiberized SA are promising to democratize pulsed mid-infrared all-fiber lasers for field applications. However, the characterization of the saturable absorption and the recovery time of the Dy^{3+}-doped silica fiber as well as the study of the behavior of this kind of mid-IR Q-switched all-fiber laser with an even lower reflectivity output coupler remain to be done to better assess the full potential of this promising system.

Funding. Natural Sciences and Engineering Research Council of Canada (CRDPJ-543631-19, IRCPJ469414-18, RGPIN2016-05877); Canada Foundation for Innovation (5180); Canada First Research Excellence Fund (Sentinel North program); CNRS - European Regional Development Fund [European Union] - Région "Provence Alpes Côte d'Azur" (PA0001777); Université Côte d'Azur (Excellence Institute JEDI), actions 6 and 10; Agence Nationale de la Recherche (ANR-15-IDEX-01).

Acknowledgments. S. Trzesien, M. Ude and B. Dussardier thank Université Côte d'Azur (through the Sentinelle Nord program) and the European FEDER/FSE Région PACA project "OPTIMAL"

Disclosures. The authors declare no conflicts of interest.

Data availability. Data underlying the results presented in this paper are not publicly available at this time but may be obtained from the authors upon reasonable request.

References

1. S. D. Jackson and R. K. Jain, "Fiber-based sources of coherent MIR radiation: key advances and future prospects (invited)," Opt. Express **28**(21), 30964–31019 (2020).
2. X. Zhu, G. Zhu, C. Wei, L. V. Kotov, J. Wang, M. Tong, R. A. Norwood, and N. Peyghambarian, "Pulsed fluoride fiber lasers at 3 μm [Invited]," J. Opt. Soc. Am. B **34**(3), A15–A28 (2017).
3. S. Jackson, M. Bernier, and R. Vallee, *MID-INFRARED FIBER PHOTONICS: Glass Materials, Fibre Fabrication and Processing, Laser Sources and Devicess* (Elsevier, 2021), chap. 7.
4. S. Duval, M. Bernier, V. Fortin, J. Genest, M. Piché, and R. Vallée, "Femtosecond fiber lasers reach the mid-infrared," Optica **2**(7), 623–626 (2015).
5. T. Hu, S. D. Jackson, and D. D. Hudson, "Ultrafast pulses from a mid-infrared fiber laser," Opt. Lett. **40**(18), 4226–4228 (2015).
6. Y. Zhou, Z. Qin, P. Yuan, J. Ma, and G. Xie, "2-MW peak-power pulses from a dispersion-managed fluoride fiber amplifier at 2.8 μm," Opt. Lett. **46**(20), 5104–5107 (2021).
7. P. Paradis, S. Duval, V. Fortin, R. Vallée, and M. Bernier, "Towards Ultrafast All-Fiber Laser at 2.8 μm Based on a SESAM and a Fiber Bragg Grating," in *2019 Conference on Lasers and Electro-Optics Europe and European Quantum Electronics Conference*, (Optical Society of America, 2019), p. cf_p_43.
8. G. Zhu, X. Zhu, F. Wang, S. Xu, Y. Li, X. Guo, K. Balakrishnan, R. A. Norwood, and N. Peyghambarian, "Graphene Mode-Locked Fiber Laser at 2.8 μm," IEEE Photonics Technol. Lett. **28**(1), 7–10 (2016).
9. S. Tokita, M. Murakami, S. Shimizu, M. Hashida, and S. Sakabe, "12 W Q-switched Er:ZBLAN fiber laser at 2.8 μm," Opt. Lett. **36**(15), 2812–2814 (2011).
10. S. Lamrini, K. Scholle, M. Schäfer, J. Ward, M. Francis, M. Farries, S. Sujecki, T. Benson, A. Seddon, A. Oladeji, B. Napier, and P. Fuhrberg, "High-Energy Q-switched Er:ZBLAN Fibre Laser at 2.79 μm," in *2015 European Conference on Lasers and Electro-Optics - European Quantum Electronics Conference*, (Optical Society of America, 2015), p. CJ_7_2.
11. L. Sojka, L. Pajewski, S. Lamrini, M. Farries, T. M. Benson, A. B. Seddon, and S. Sujecki, "High Peak Power Q-switched Er:ZBLAN Fiber Laser," J. Lightwave Technol. **39**(20), 6572–6578 (2021).
12. X. Lai, J. Li, H. Luo, C. Zhu, Y. Hai, Y. Shi, Y. Gao, and Y. Liu, "High power passively Q-switched Er^{3+}-doped ZBLAN fiber laser at 2.8 μm based on a semiconductor saturable absorber mirror," Laser Phys. Lett. **15**(8), 085109 (2018).
13. Y. Wang and H. Luo, "Wavelength-tunable, linearly polarized Q-switched and gain-switched polarization-maintaining Er^{3+}-doped fluoride fiber laser in the range of 2.7~2.83 μm," Opt. Commun. **504**, 127482 (2022).
14. Y. O. Aydin, S. Magnan-Saucier, D. Zhang, V. Fortin, D. Kraemer, R. Vallée, and M. Bernier, "Dual stage fiber amplifier operating near 3 μm with milijoule-level, sub-ns pulses at 5 W," Opt. Lett. **46**(18), 4506–4509 (2021).
15. K. Zhang, I. Alamgir, and M. Rochette, "Midinfrared Compatible Tunable Bandpass Filter Based on Multimode Interference in Chalcogenide Fiber," J. Lightwave Technol. **38**(4), 857–863 (2020).
16. P. Paradis, V. Fortin, Y. O. Aydin, R. Vallée, and M. Bernier, "10 W-level gain-switched all-fiber laser at 2.8 μm," Opt. Lett. **43**(13), 3196–3199 (2018).
17. G. Bharathan, L. Xu, X. Jiang, H. Zhang, Z. Li, F. Chen, and A. Fuerbach, "MXene and $PtSe_2$ saturable absorbers for all-fibre ultrafast mid-infrared lasers," Opt. Mater. Express **11**(7), 1898–1906 (2021).
18. A. Kurkov, "Q-switched all-fiber lasers with saturable absorbers," Laser Phys. Lett. **8**(5), 335–342 (2011).
19. L. Tordella, H. Djellout, B. Dussardier, A. Saïssy, and G. Monnom, "High repetition rate passively Q-switched Nd^{3+}:Cr^{4+} all-fibre laser," Electron. Lett. **39**(18), 1307–1308 (2003).

Optics EXPRESS

20. B. Dussardier, J. Maria, and P. Peterka, "Passively Q-switched ytterbium- and chromium-doped all-fiber laser," Appl. Opt. **50**(25), E20–E23 (2011).
21. A. Fotiadi, A. Kurkov, and I. Razdobreev, "All-fiber passively Q-switched ytterbium laser," in *CLEO/Europe. 2005 Conference on Lasers and Electro-Optics Europe, 2005*., (2005), p. 515.
22. S. D. Jackson, "Passively Q-switched Tm^{3+}-doped silica fiber lasers," Appl. Opt. **46**(16), 3311–3317 (2007).
23. A. Kurkov, E. Sholokhov, and O. Medvedkov, "All fiber Yb-Ho pulsed laser," Laser Phys. Lett. **6**(2), 135–138 (2009).
24. J.-F. Lupi, M. Vermillac, S. Trzesien, M. Ude, W. Blanc, and B. Dussardier, "Gradual-time solution doping for the fabrication of longitudinally varying optical fibres," J. Lightwave Technol. **36**(10), 1786–1791 (2018).
25. J. Townsend, S. Poole, and D. Payne, "Solution-doping technique for fabrication of rare-earth-doped optical fibres," Electron. Lett. **23**(7), 329–331 (1987).
26. T. Izawa, N. Shibata, and A. Takeda, "Optical attenuation in pure and doped fused silica in the ir wavelength region," Appl. Phys. Lett. **31**(1), 33–35 (1977).
27. L. Verre Fluoré, "Fiber Solutions - Le Verre Fluoré," (2021). https://leverrefluore.com/.
28. O. Humbach, H. Fabian, U. Grzesik, U. Haken, and W. Heitmann, "Analysis of OH absorption bands in synthetic silica," J. Non-Cryst. Solids **203**, 19–26 (1996).
29. J. M. F. van Dijk and M. F. H. Schuurmans, "On the nonradiative and radiative decay rates and a modified exponential energy gap law for 4f–4f transitions in rare-earth ions," J. Chem. Phys. **78**(9), 5317–5323 (1983).
30. R. Reisfeld, "Radiative and non-radiative transitions of rare-earth ions in glasses," in *Rare Earths*, (Springer, 1975), pp. 123–175.
31. L. Luo and P. Chu, "Passive Q-switched erbium-doped fibre laser with saturable absorber," Opt. Commun. **161**(4-6), 257–263 (1999).
32. L. Gomes, A. F. H. Librantz, and S. D. Jackson, "Energy level decay and excited state absorption processes in dysprosium-doped fluoride glass," J. Appl. Phys. **107**(5), 053103 (2010).
33. D. J. Maas, B. Rudin, A.-R. Bellancourt, D. Iwaniuk, S. V. Marchese, T. Südmeyer, and U. Keller, "High precision optical characterization of semiconductor saturable absorber mirrors," Opt. Express **16**(10), 7571–7579 (2008).
34. J. Habel, T. Boilard, J.-S. Frenière, F. Trépanier, and M. Bernier, "Femtosecond FBG Written through the Coating for Sensing Applications," Sensors **17**(11), 2519 (2017).
35. S. Cozic, S. Boivinet, C. Pierre, J. Boulet, S. Poulain, and M. Poulain, "Splicing fluoride glass and silica optical fibers," EPJ Web Conf. **215**, 04003 (2019).
36. J. Swiderski and M. Michalska, "Generation of self-mode-locked resembling pulses in a fast gain-switched thulium-doped fiber laser," Opt. Lett. **38**(10), 1624–1626 (2013).
37. S. Magnan-Saucier, S. Duval, C. Matte-Breton, Y. O. Aydin, V. Fortin, S. LaRochelle, M. Bernier, and R. Vallée, "Fuseless side-pump combiner for efficient fluoride-based double-clad fiber pumping," Opt. Lett. **45**(20), 5828–5831 (2020).